

Characteristics of Supercritical Turbulence from Direct Numerical Simulations of C_7H_{16}/N_2 and O_2/H_2 Temporal Mixing Layers

Nora A. Okong'o and Josette Bellan*

Jet Propulsion Laboratory, California Institute of Technology, Pasadena, CA 91109-8099

Abstract

Analysis of Direct Numerical Simulations (DNS) transitional states of temporal, supercritical mixing layers for C_7H_{16}/N_2 and O_2/H_2 shows that the evolution of all layers is characterized by the formation of high-density-gradient magnitude (HDGM) regions. Due to the specified, smaller initial density stratification, the C_7H_{16}/N_2 layers display higher growth and increased global molecular mixing as well as larger turbulence levels than comparable O_2/H_2 layers. However, the O_2/H_2 layer exhibits an enhanced local mixing resulting from the increased mixture solubility and from mixture near-ideality. These thermodynamic features lead to a larger irreversible entropy production (dissipation) in O_2/H_2 versus C_7H_{16}/N_2 layers. The largest O_2/H_2 dissipation is concentrated in HDGM regions that are distortions of the initial density stratification boundary, whereas the largest C_7H_{16}/N_2 dissipation is located in HDGM regions resulting from fluid mixing.

Introduction

Past the critical point of a fluid (where material liquid-vapor surfaces no longer exist), jets injected through an orifice no longer atomize as in sprays [1] but instead disintegrate and assume the aspect of what Chehroudi et al. [2] call 'fingers', or 'comb-like structures' at transcritical conditions, having an increasingly gaseous appearance with increasing pressure p ; these experiments were conducted with N_2/N_2 , $N_2/(CO+N_2)$, He/N_2 and O_2/N_2 . Similar experimental observations were reported by Mayer et al. [3, 4] for O_2 disintegration. Raman scattering measurements of the radial density in free N_2 jets at 4 MPa by Oswald and Schik [5] showed sharp profiles independent of the injection temperature, indicating the occurrence of sharp density gradients. Regions of high density-gradient-magnitude (acronym HDGM) were also shown to exist in Direct Numerical Simulations (DNS) of both pre-transitional [6] and transitional [7, 8] supercritical binary-species mixing layers. These HDGM regions were found to be the venues for high dissipation (irreversible entropy production) [7, 8], with most of the dissipation due to species-mass flux and minimal dissipation from viscous effects. The location of the highest dissipation in the HDGM regions was attributed to the sharp density stratification being very effective at damping turbulent eddies [9, 10], because it is qualitatively similar to a rigid flat plate. However, there is still uncertainty about how these features, separately ob-

tained for two different binary-species systems, compare on a non-dimensional basis. The comparison of these features for the two binary-species systems is the subject of this study.

Highlights of the supercritical DNS

The conservation equations originate in Keizer's [11] fluctuation-dissipation theory which is consistent with non-equilibrium thermodynamics, converges to kinetic theory in the low-pressure limit and relates fluxes and forces from first principles. There are three primary differences between existing mixing-layer low-pressure equations and the equations used to generate the present database: (1) The flux matrix here contains Soret and Dufour effects in the species-mass and heat fluxes, respectively, in addition to Fick's diffusion and Fourier terms. This means that both of these fluxes contain terms that are proportional to ∇T (where T is the temperature), ∇Y (where Y is the species mass fraction), and ∇p (see details in [7, 8]). (2) p is calculated from the well-known Peng-Robinson equation of state (EOS). Consistently, all thermodynamic quantities are calculated from the EOS, including the important mass diffusion coefficient, α_D , which measures the mixture non-ideality. α_D multiplies the diffusivity D in the Fick's term, thereby modifying the species diffusivity; for ideal mixtures $\alpha_D = 1$ and the low-pressure perfect-gas situation is recovered, however, for non-ideal mixtures $0 \leq \alpha_D < 1$,

*Corresponding author: josette.bellan@jpl.nasa.gov. Proceedings of the Third Joint Meeting of the U.S. Sections of The Combustion Institute

which means that species diffusion is impeded compared to perfect gases. (3) The viscosity μ , the Schmidt number and the Prandtl number were calculated from high-pressure single-species transport properties using mixing rules, as in Harstad and Bellan [12]. The calculated values were correlated as functions of the thermodynamic variables, and these correlations were then used to compute the transport properties D and λ .

The temporally developing mixing layer is depicted in Fig. 1 for O_2/H_2 , as an example, showing the streamwise (x_1), cross-stream (x_2) and spanwise (x_3) coordinates. The layer is not x_2 -symmetric in extent so as to accommodate the larger growth in the lighter fluid (H_2 or N_2) side. The free-stream density (ρ_1 or ρ_2) is calculated for each pure species at its free-stream temperature (T_1 or T_2) and at the initial uniform pressure (p_0). The vorticity thickness is defined as $\delta_\omega(t) = \Delta U_0 / (\partial \langle u_1 \rangle / \partial x_2)_{max}$ where $\langle u_1 \rangle$ is the (x_1, x_3) planar average of the streamwise velocity, and $\Delta U_0 = U_1 - U_2$ is the velocity difference across the layer. The simulations were initiated with four streamwise and spanwise vortices, and a vorticity perturbation of wavelength λ_1 and of amplitude F_{2D} in the streamwise direction and F_{3D} in the spanwise direction induced two pairings to produce an ultimate vortex. U_1 and U_2 are functions of the ratio of the speeds of sound of the free streams, of ρ_1/ρ_2 , possibly of Z_1/Z_2 where $Z = p / (\rho T R_u / m)$ is the compression factor which indicates departures from perfect gas ($Z = 1$) behavior (R_u is the universal gas constant and m is the mixture molar weight), and of the convective Mach number $M_{c,0}$ whose specification therefore determines ΔU_0 . Given the initial streamwise velocity profile u_1 based on U_1 and U_2 , $(\partial \langle u_1 \rangle / \partial x_2)_{max}$ and hence $\delta_{\omega,0} \equiv \delta_\omega(0)$ are calculated. The specified value of the initial flow Reynolds number, $Re_0 = [0.5(\rho_1 + \rho_2)\Delta U_0\delta_{\omega,0}] / \mu_R$, is then used to calculate μ_R . Careful considerations regarding matching of the initial conditions between the two binary-species systems while still addressing regimes of practical interest [13] leads to the matching of the reduced pressure $p_r = p/p_c$ of the heavier fluid and of the momentum ratio of the layers as shown in Table 1 listing all simulations considered. The layers were perturbed either at the incompressible most unstable wavelength $\lambda_1/\delta_{\omega,0} = 7.29$, or at the compressible most unstable wavelength (10.61 or 10.35), or at the estimated smallest unstable wavelength (4.57), all obtained from an inviscid linear analysis.

The conservation equations were numerically solved using fourth-order explicit Runge-Kutta time integration and a sixth-order compact scheme with eighth-order filter for spatial derivatives; for numerical stability, filtering is applied at interior points only. The computations were par-

allelized using three-dimensional domain decomposition and message passing, and an efficient parallel tridiagonal solver.

Global Growth and Mixing

A fundamental characteristic of mixing layers is their growth, which can be measured using the momentum thickness, here defined as

$$\delta_m = \frac{-1}{(\theta_1 - \theta_2)^2} \int_{-L_{2,\min}}^{L_{2,\max}} (\theta_2 + \langle \rho u_1 \rangle) (\theta_1 + \langle \rho u_1 \rangle) dx_2 \quad (1)$$

with $\theta_1 = \langle \rho u_1 \rangle_{x_2=L_{2,\max}}$ and $\theta_2 = \langle \rho u_1 \rangle_{x_2=L_{2,\min}}$, where $L_{2,\min} = -L_2/3$ and $L_{2,\max} = 2L_2/3$. While the growth is mostly a consequence of entrainment, the product thickness defined as $\delta_p = \int \int \int_V \rho Y_p dV$ in mass units, where $Y_p = 2 \min(Y_1, Y_2)$, is a direct consequence of molecular mixing. $\delta_m/\delta_{\omega,0}$ is illustrated as a function of the non-dimensional time $t^* = t\Delta U_0/\delta_{\omega,0}$ in Fig. 2(a) for all simulations. All layers roll up and pair twice, however, the C_7H_{16}/N_2 layers display a drastic increase in $\delta_m/\delta_{\omega,0}$ after the first pairing, whereas their O_2/H_2 counterpart tend to grow more slowly. The drastic growth of the C_7H_{16}/N_2 layers compared to the O_2/H_2 ones is attributed to the smaller initial density stratification of the former. Not surprisingly, $\delta_p/\delta_{p,0}$, depicted in Fig. 2(b) displays a much larger growth for C_7H_{16}/N_2 than for O_2/H_2 as a function of t^* , meaning that global molecular mixing is much more intense. Illustrated in Fig. 2(c) is the non-dimensional positive spanwise vorticity, $\langle \langle \omega_3^+ \rangle \rangle (\delta_{\omega,0}/\Delta U_0)$, which is indicative of small turbulent scale formation considering that due to the initial mean velocity profile, the initial spanwise vorticity is negative. The non-dimensional enstrophy, $\langle \langle \omega_i \omega_i \rangle \rangle (\delta_{\omega,0}/\Delta U_0)^2$, where $\langle \langle \rangle \rangle$ denotes volume averaging, is shown in Fig. 2(d) and is a manifestation of stretching and tilting, which is the mechanism primarily responsible for the formation of small scales. For all simulations, $\langle \langle \omega_3^+ \rangle \rangle (\delta_{\omega,0}/\Delta U_0)$ increases from the null value once the layer roll-up is completed; for each of the set of species, the layer perturbed at the shortest wavelength exhibits the earliest roll-up and highest $\langle \langle \omega_3^+ \rangle \rangle (\delta_{\omega,0}/\Delta U_0)$ maximum growth. Noticeably, the two O_2/H_2 layers perturbed at the most unstable wavelength and having a smaller Re_0 display a delayed roll-up with respect to all other layers. Comparing the O_2/H_2 and C_7H_{16}/N_2 layers, one observes a drastically reduced $\langle \langle \omega_3^+ \rangle \rangle (\delta_{\omega,0}/\Delta U_0)$ augmentation rate for the former compared to the latter (with particular significance for the OH500 and HN500 layers, which have the same Re_0) indicating a reduced layer growth rate. All curves exhibit local peaks at the first pairing; however, $\langle \langle \omega_3^+ \rangle \rangle (\delta_{\omega,0}/\Delta U_0)$ increases following the first pairing of

the C_7H_{16}/N_2 layers but decreases for the O_2/H_2 layers. Moreover, $\langle \langle \omega_3^+ \rangle \rangle (\delta_{\omega,0}/\Delta U_0)$ is considerably smaller for the O_2/H_2 layer compared to the equivalent C_7H_{16}/N_2 ones, indicating that turbulence for the former is substantially reduced with respect to the latter. The enstrophy variation is consistent with this physical picture, displaying reduced levels for the O_2/H_2 layers when compared to the C_7H_{16}/N_2 ones. The largest enstrophy among O_2/H_2 layers corresponds to the one exhibiting the earliest roll-up and maximum positive spanwise vorticity.

Turbulence and Dissipation

Depicted in Fig. 3 is $|\nabla\rho| \delta_{\omega,0}/\Delta\rho_0$ for the layers listed in Table 1, in the braid planes at the respective transitional times. All contour plots depict only the significant portion of the computational domain in the x_2 direction and the $|\nabla\rho| \delta_{\omega,0}/\Delta\rho_0$ contour levels range from 10% to 90% of the highest value in the domain. Species-system-dependent aspects can be discerned by comparing HN600 (Fig. 3(d)) and OH750 (Fig. 3(e)), which have a similar magnitude of $Re_{m,tr}$ and are excited with the same $\lambda_1/\delta_{\omega,0}$ and F_{3D} (see Table 1). Although the OH750 layer is initiated with about the same $|\nabla\rho| \delta_{\omega,0}/\Delta\rho_0$ value (albeit with about twice the density stratification) of HN600, $|\nabla\rho| \delta_{\omega,0}/\Delta\rho_0$ at transition is about a factor of 2 smaller than that of HN600. The larger $|\nabla\rho| \delta_{\omega,0}/\Delta\rho_0$ value for the HN600 layer is due to the increased non-ideality of the C_7H_{16}/N_2 mixture (i.e. $0.5 < \alpha_D < 1$ [7]), which impedes molecular mixing when compared to the O_2/H_2 mixture (i.e. $\alpha_D \sim 1$ [8]). Independent of the initial conditions, individual HDGM regions in the O_2/H_2 layers exhibit a greater spatial extent than their C_7H_{16}/N_2 counterpart, which results from the combined effect of the much larger solubility of H_2 into O_2 than of N_2 into C_7H_{16} and of the much better molecular mixing of O_2/H_2 . Thus, non-ideality manifests itself both through increased value of $|\nabla\rho| \delta_{\omega,0}/\Delta\rho_0$ (labelled ‘stronger’ HDGM regions) and through narrower individual HDGM regions. Comparing the other layers in Fig. 3, it is apparent that $|\nabla\rho| \delta_{\omega,0}/\Delta\rho_0$ increases with Re_0 at otherwise similar initial conditions (HN500 versus HN600; OH500 versus OH550). For same C_7H_{16}/N_2 initial conditions (HN500 versus HN600), the HDGM regions are distributed over a larger portion of the domain with increasing Re_0 . The much larger $|\nabla\rho| \delta_{\omega,0}/\Delta\rho_0$ values of the HN800 layer are attributed to the decreased characteristic time of the flow, induced by the larger Re_0 , which leads to a reduced ratio of the distortion time to the molecular mixing time. The more convoluted structure of the HN500 layer compared to the HN800 layer, despite being the same species at similar $Re_{m,tr}$, results from the relative ease in distorting the weaker HDGM regions in the former simula-

tion.

Okong’o and Bellan [14] have shown that if g denotes the rate of irreversible entropy production for a single-phase binary-species flow devoid of sources or sinks, then $g = g_{visc} + g_{temp} + g_{mass}$, where the three contributions stem from viscous, Fourier heat and species-mass fluxes. Plots of g at the respective transitional times (illustrated in [13]) show that all layers display localized regions of high dissipation which are located in the HDGM regions. However, whereas the highest g magnitude regions are observed in the lower stream for the OH layers, the HN layers exhibit the highest g magnitude regions in the upper stream. That is, for the HN layers, the largest dissipation occurs in the upper stream, which has lighter fluid, within HDGM regions originating from fluid mixing rather than the original density stratification and therefore have high $|\nabla Y|$ but relatively low $|\nabla\rho|$; therefore, this mechanism can be partially attributed to the mixture non-ideality, which is a thermodynamic effect. Although this mechanism is also active in the OH layers, it is no longer the dominant one. Because the O_2/H_2 mixture is very nearly ideal, the major contribution to the dissipation is there from the lower layer regions, located in the heavier fluid, which originate from the distortion of the initial density stratification boundary and have high $|\nabla\rho|$ but low $|\nabla Y|$; therefore, this mechanism is dynamic in origin.

Conclusions

Databases obtained from DNS of binary-species supercritical temporal mixing layers were compared at the respective transitional states to investigate the species-dependent aspects of supercritical turbulence. The analysis involved comparisons among six simulations, three of which were for O_2/H_2 and three others for C_7H_{16}/N_2 layers; in all cases the heavier fluid was in the lower stream. All simulations were performed at similar reduced pressure and layer initial momentum ratio. For these conditions, the initial density stratification of the O_2/H_2 layers was almost twice that of the C_7H_{16}/N_2 layers. Global characteristics of the six layers showed that the momentum thickness and product thickness growth is substantially reduced for the O_2/H_2 layers compared to the C_7H_{16}/N_2 ones, and that the levels of the positive spanwise vorticity and the enstrophy for the O_2/H_2 layers were also diminished, indicating less turbulence activity. These results are attributed to the much larger initial density stratification of the O_2/H_2 layers, which delays entrainment and pairing. All layers displayed high density-gradient magnitude regions at transition, which form due both to the distortion of the initial density stratification boundary and to the mixing of the species, and all layers exhibited high mass-

fraction gradient regions. Most of the dissipation activity occurred in these high density-gradient magnitude and high mass-fraction gradient regions; however, the largest dissipation is located for the O_2/H_2 layers within regions originating from the distortion of the original density stratification boundary, and for the C_7H_{16}/N_2 layers within regions created through mixing. The maximum dissipation level is larger for the O_2/H_2 layer, consistent with the lower turbulence levels detected from the global analysis. Thus, for supercritical mixing layers, we identified structures (high density-gradient and high mass-fraction-gradient regions) and thermodynamic processes (solubility and mixture ideality) that affect turbulence development.

Acknowledgements

This work was conducted at the Jet Propulsion Laboratory (JPL), California Institute of Technology and sponsored by the National Aeronautics and Space Administration (NASA), Marshall Space Flight Center under the direction of Dr. John Hutt, by the Air Force Office of Scientific Research under the direction of Dr. Julian Tishkoff, and by the Army Research Office under the direction of Dr. David Mann, through interagency agreements with NASA. The computational resources were provided by the JPL Supercomputing Center.

References

- [1] Bellan, J., *Progress in Energy and Combustion Science* 26(4-6):329-366 (2000).
- [2] Chehroudi, B., Talley, D., and Coy, E., AIAA Paper 99-0206, AIAA Thirty-Seventh Aerospace Sciences Meeting and Exhibit, Reno, NV, Jan. 11-14, 1999.
- [3] Mayer, W., Schik, A., Schweitzer, C., and Schaffler, M., AIAA Paper 96-2620, AIAA/ASME/SAE/ASEE

Thirty-Second Joint Propulsion Conference, Lake Buena Vista, FL, July 1-3, 1996.

- [4] Mayer, W., Ivancic, B., Schik, A., and Hornung, U., AIAA Paper 98-3685, AIAA/ASME/SAE/ASEE Thirty-Fourth Joint Propulsion Conference and Exhibit, Cleveland, OH, July 13-15, 1998.
- [5] Oschwald, M., and Schik A., *Experiments in Fluids* 27:497-506 (1999).
- [6] Miller, R., Harstad, K., and Bellan, J., *Journal of Fluid Mechanics* 436:1-39 (2001).
- [7] Okong'o, N., and Bellan, J., *Journal of Fluid Mechanics* 464:1-34 (2002).
- [8] Okong'o, N., Harstad, K., and Bellan, J., *AIAA Journal* 40(5):914-926 (2002).
- [9] Hannoun, I., Fernando, H., and List, E., *Journal of Fluid Mechanics* 189:189-209 (1988).
- [10] Briggs, D., Ferziger, J., Koseff, J., and Monismith, S., *Journal of Fluid Mechanics* 354:175-208 (1998).
- [11] Keizer, J., *Statistical Thermodynamics of Nonequilibrium Processes*. Springer-Verlag, New York, 1987.
- [12] Harstad K., and Bellan, J., *International Journal of Heat and Mass Transfer* 41:3537-3550 (1998).
- [13] Okong'o, N., and Bellan, J., Turbulence and area production in binary-species, supercritical, transitional mixing layers, submitted to *Physics of Fluids* (2003).
- [14] Okong'o, N., and Bellan, J., *Proceedings of the Combustion Institute*, Vol. 28, The Combustion Institute, Pittsburgh, 2000, pp. 497-504.

Run	Re_0	ρ_2/ρ_1	$\lambda_1/\delta_{\omega,0}$	F_{3D}	$L_1 \times L_2 \times L_3$	$N_1 \times N_2 \times N_3$	$Re_{m,tr}$	t_{tr}^*	CPU(h)
OH500	500	24.51	10.61	0.025	0.291×0.291×0.1746	352×352×208	1772	290	14557
OH550	550	24.40	10.35	0.025	0.284×0.284×0.17	352×352×208	1907	270	14497
OH750	750	24.40	7.29	0.05	0.2×0.2×0.12	352×352×208	1507	150	10349
HN500	500	12.88	7.29	0.05	0.2×0.232×0.12	240×288×144	1250	155	1714
HN600	600	12.88	7.29	0.05	0.2×0.232×0.12	288×336×176	1452	135	5156
HN800	800	12.88	4.57	0.05	0.125×0.148×0.075	240×272×144	1258	100	1916

Table 1: Listing of the simulations and associated resolution for O_2/H_2 (OH) and C_7H_{16}/N_2 (HN) mixing layers. L_i is in meters. For all layers, $M_{c,0} = 0.4$, $L_1=4\lambda_1$, $\delta_{\omega,0}=6.859 \times 10^{-3}$ m and $F_{2D}=0.1$. The other initial conditions are: $p_0=100$ atm (OH), 60atm (HN); $p_r=2.01$ (O_2), 2.22 (C_7H_{16}); $T_1=287$ K (OH500), 600K (OH550, OH750), 1000K (HN); $T_2=235$ K (OH500), 400K (OH550, OH750), 600K (HN); $|\rho_2 U_2|/|\rho_1 U_1|=4.951$ (OH500), 5.001 (OH550, OH750), 5.276 (HN). The subscript tr denotes the transitional time. The CPU time is based on an SGI Origin2000 300MHz R12000 processor.

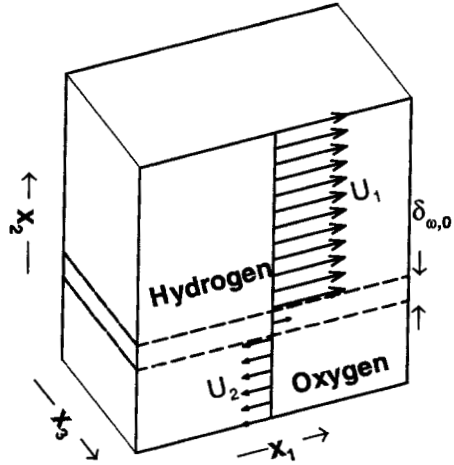


Figure 1: Sketch of the O_2/H_2 mixing layer configuration.

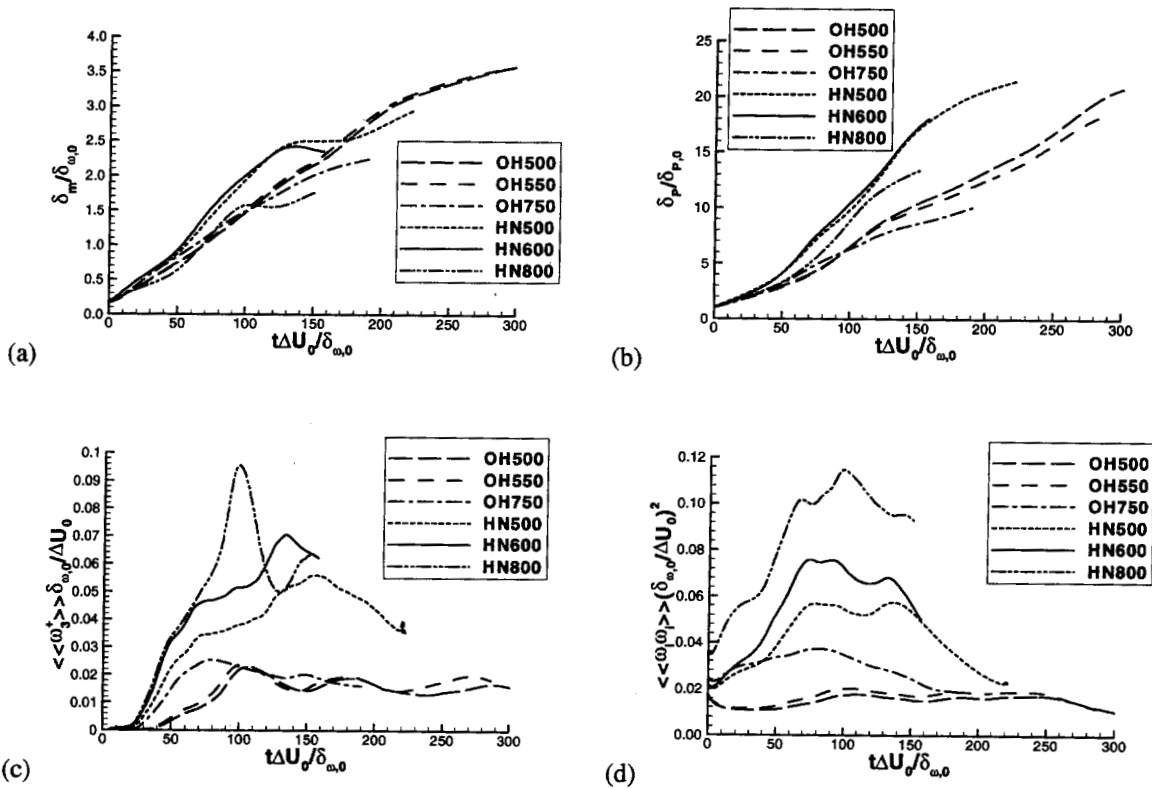


Figure 2: Non-dimensionalized (a) momentum thickness, (b) product thickness, (c) global positive spanwise vorticity, and (d) enstrophy, all versus $t^* = t / (\Delta U_0 / \delta_{\omega,0})$.

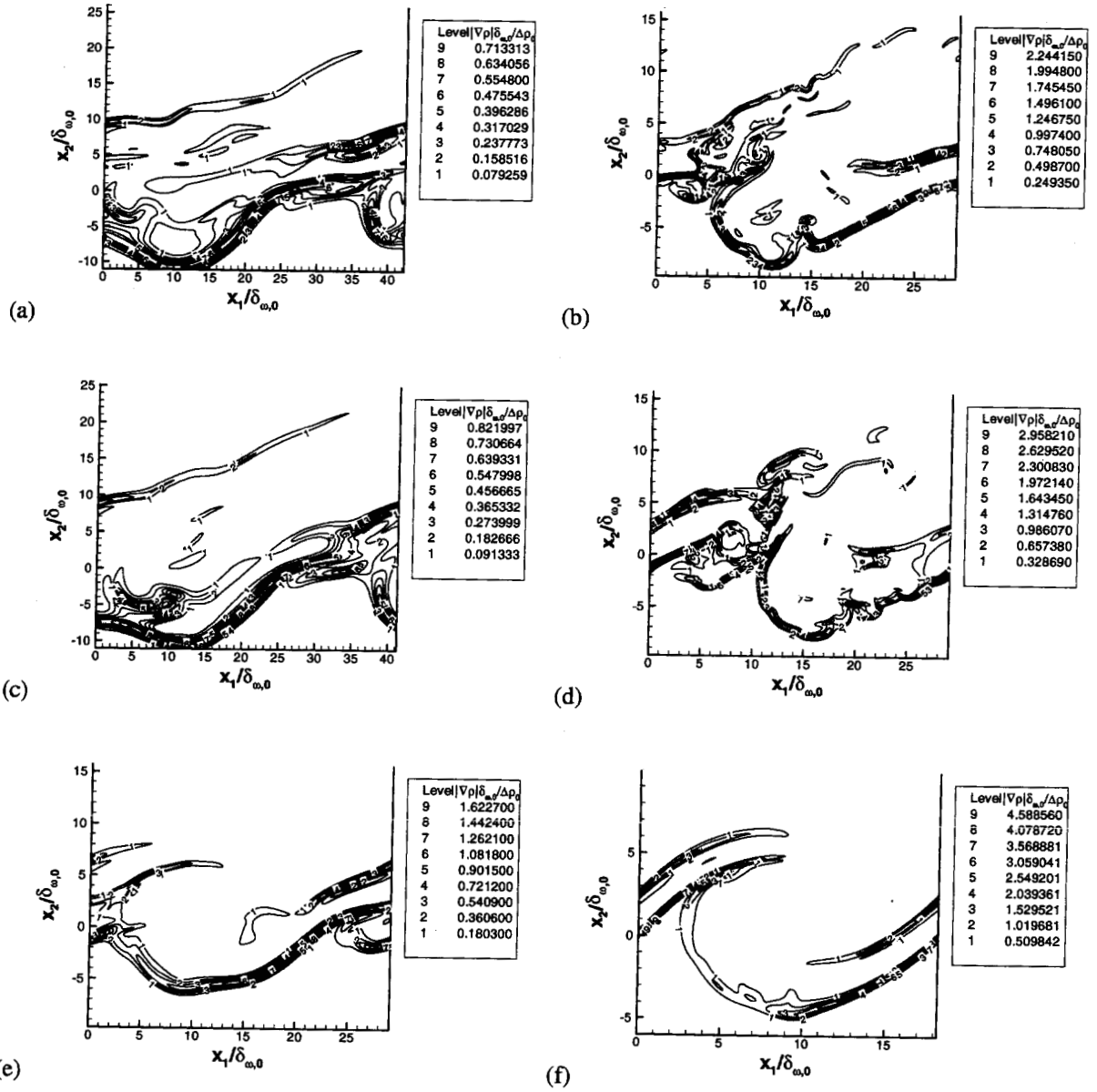


Figure 3: Density gradient magnitude for (a) OH500, (b) HN500, (c) OH550, (d) HN600, (e) OH750 and (f) HN800: in the braid plane ($x_3 = L_3/16$).